THE JOURNAL OF PHYSICAL CHEMISTRY C
A JOURNAL OF THE AMERICAN CHEMICAL SOCIETY

pubs.acs.org/JPCC

Article

Hydration Structure of Diamondoids from Reactive Force Fields

Karol Palczynski,* Thorren Kirschbaum,* Annika Bande,* and Joachim Dzubiella*

Cite This: J. Phys. Chem. C 2023, 127, 3217−3227

Read Online

ACCESS | Metrics & More | Article Recommendations | Supporting Information

ABSTRACT: Diamondoids are promising materials for applications in catalysis and nanotechnology. Since many of their applications are in aqueous environments, to understand their function it is essential to know the structure and dynamics of the water molecules in their first hydration shells. In this study, we adapt a reactive force field (ReaxFF) for atomistically resolved molecular dynamics simulations of hydrated diamondoids to characterize their interfacial water structure. We parametrize the force field and validate the water structure against geometry-optimized structures from density functional theory. We compare the results to water structures around diamondoids with all partial charges set to zero, and around charged smooth spheres, and find qualitatively similar water structuring in all cases. However, the response of the water molecules is most sensitive to the partial charges in the atomistically resolved diamondoids. From the systematic exclusion of atomistic detail, we can draw generic conclusions about the nature of the hydrophobic effect at nanoparticle interfaces and link it to the interfacial water structure. The interactions between discrete partial charges on short length scales affect the hydration structures strongly, but the hydrophobic effect seems to be stable against these short scale surface perturbations. Our methods and the workflow we present are transferable to other hydrocarbons and interfacial systems.

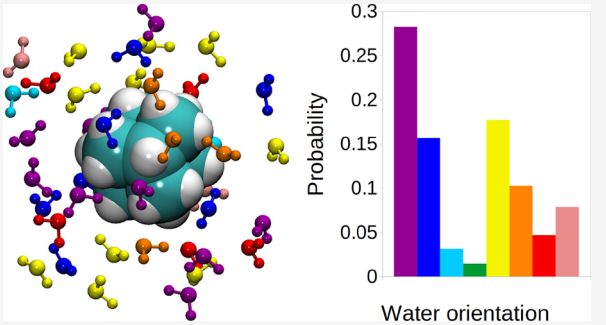

1. INTRODUCTION

Nanodiamonds (NDs) are nanometer-sized undoped, hydrogen terminated fragments of the diamond crystal lattice. The smallest NDs form a subclass called diamondoids (DDs), also named polymantanes, which are constructed from the smallest unit cage structure of the diamond lattice, the molecule adamantane (AD) with the molecular formula $C_{10}H_{16}$. DDs and NDs are an important class of hydrocarbons with applications in nanotechnology[1−6] and biomedicine,[7−10] due to their physical stability, chemical inertness and high surface-to-volume ratio.[11−13] For many applications, the molecules are solvated in aqueous media. The interactions between the water molecules and the diamond-based solutes as well as the structure of the water molecules at the solute−water interfaces significantly affect the function of these materials.[14] However, the nanoscale hydration structures of hydrogenated NDs and DDs are still under debate.

In experiments, the interfacial water molecules around NDs of various surface terminations have been probed using X-ray absorption,[15,16] infrared[12,16,17] or Raman, and photoluminescence[18] spectroscopy, as well as differential scanning calorimetry[12] or Fabry−Perot interferometry.[19] However, all these methods leave much room for interpretation as direct imaging of the interfacial water molecules is not yet possible.[20,21] Other related studies shed some light on the water structure by combining experiments and computer simulations of water around hydrophobic solutes.[20] Classical atomistic molecular dynamics (MD) computer simulations provide an idealized model of hydrated NDs and DDs. The hydration properties of the solutes depend significantly on the electrostatic interactions, which in MD simulations are governed by the Coulomb potential, and so they depend on the partial charges on the atoms of the hydrated molecules.[22−25] There are many different approaches for implementing partial charges in MD simulations. A critical difference between all methods is that either the charges on the atoms are fixed, i.e., constant in time, or the atoms are polarizable, so that the charges respond to their environments. Both ways have been applied in MD simulations of NDs and DDs. We will next review studies that used fixed partial charges, then experiments, and then simulations with polarizable charges.

Fixed partial charges are still the standard in MD simulations. For instance, fixed partial charges have been used to simulate the distribution and dynamics of functionalized AD molecules in a lipid bilayer.[26] Combined with classical force fields, the AD charges (with implicit hydrogens) were obtained from quantum density functional theory (DFT) calculations. Others have investigated the surface charge density from the zeta potential of an ND slab in water using a classical force field.[27] The partial

Received: November 4, 2022
Revised: January 20, 2023
Published: February 6, 2023

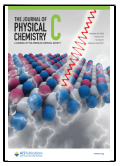

charges were calculated with the so-called extended bond-charge increment scheme.[28] In yet other studies, default partial charges implemented in simulation software packages have been used to simulate binding of NDs to supramolecular structures.[29,30] Of particular importance for the present work are studies that report properties of hydrated AD molecules. Two studies have simulated density distributions and orientations of water molecules around AD monomers[31] and dimers.[32] These studies found that the water molecules in the first hydration shells are mostly oriented tangential to the AD surface. In another study, thermodynamic hydration properties for the AD molecule and bigger DDs have been calculated from MD.[22] As most did before, the authors used classical force fields and the fixed partial charges were calculated with DFT. The MD simulations reveal that the enthalpy of hydration is negative, but it is compensated by the entropic contribution to the hydration free energy. However, the balance between enthalpy and entropy sensitively depends on the force field. Some force fields with fixed nonzero charges yield negative hydration free energies, which is inconsistent with the low water solubilities of DDs observed in experiments,[22] whereas, when all solute charges are set to zero, AD molecules are clearly hydrophobic.[33]

Experiments confirm the hydrophobic character of DDs. Measurements of DD solubilities in pressurized hot water showed that DDs are less soluble in water (i.e., more hydrophobic) than most aromatic hydrocarbons of the same carbon number.[34] For instance, at 313 K and 500 atm, the aqueous solubility of AD is 240 times lower than that of naphthalene. This effect can be emphasized by the tendency of the DDs to nucleate in water due to strong van der Waals interactions between them.[22] However, the authors of the experiments state that nucleation did not affect the resulting solubility values. Measurements of thermodynamic properties of host−guest complexation with DDs also agree that DDs are strongly hydrophobic.[35−37] Interestingly, X-ray absorption and Raman measurements of small hydrogenated NDs[16] suggest that they are disrupting the water hydrogen bond network surrounding them. A decrease of the OH bending vibrational mode reveals the presence of non-hydrogen bonded water OH groups in the first hydration shell. These OH groups seem to be associated with the hydrogenated ND surface groups. Non-hydrogen bonded OH groups in the hydration shells of hydrophobic solutes, including NDs, have been discussed in earlier studies.[24,38−43] Close to the interface, a significant amount of water molecules points with their OH groups toward the hydrophobic interface, where the water molecules take on a slightly ice-like order.[43] The probability for the formation of non-hydrogen bonded OH bonds depends, among others, on the solute's charge.[42] Under certain conditions, i.e., if a solute contains polar groups, water molecules can also take part in weak C−H···O−H_2 hydrogen bonds,[38] which can have a high influence on molecular conformations.[44] Experimentally, however, C−H···O−H_2 bonds are difficult to confirm and to distinguish from conventional water−water hydrogen bonds.[38] Raman measurements of NDs show no traces of CH surface groups forming hydrogen bonds with water molecules.[16] Hydrogenated NDs and DDs are strongly hydrophobic, but quantum calculations show that the binding energy of a single water molecule to AD in a vacuum is 0.92 kcal/mol,[31] very weak compared to the water−water hydrogen bond strength of 5.5 kcal/mol in bulk water at normal conditions,[45] but not negligible.

For classical force fields to be able to replicate the physics of hydrated DDs, MD simulations may require the use of force fields that explicitly address the effects of electrostatic polarization to incorporate a higher level of realism.[22] One work analyzed the effects of ND additives on the adsorption of tricresyl phosphate on iron oxide surfaces.[3] The authors used the ReaxFF force field with a parameter set optimized for interactions between hydrocarbons and metals in water.[46,47] The partial charges were calculated with a charge equilibration method (QEq).[48−51] A related method was used to calculate the partial charges of AD and bigger DDs for interactions with biopolymers in water.[4,52] There is no consensus on a force field for the simulation of NDs and DDs, or in particular for the interactions between DDs and water. The hydration structure of NDs and DDs has not yet been studied with polarizable partial charges. For that purpose, the QEq method seems promising, but it requires a carefully chosen set of parameters. Additionally, the ReaxFF force field will enable us to study reactive surface chemistry, such as reactions of graphitic carbon with water,[53−55] solvated electrons[56−58] (through eReaxFF, e.g., ref 59), and the influence of surface modifications,[60−63] in the future. For simulations of hydrocarbons in water, there are three notable QEq parameter sets for the ReaxFF force field published in literature. The "Aryanpour" parameter set was first designed for interactions between hydrocarbons and metals[64] and later extended to work well in water.[47] The "Wang" parameter set can describe chemical reactions of C- and Si-based solids with water, H_2, and O_2 molecules.[65] The "Zhang" parameter set not only focuses primarily on the correct bulk water structure and dynamics of water molecules in the condensed phase but also considers the weak interactions between hydrocarbons and water.[66]

The goal of this study is to find a ReaxFF force field that is able to reproduce the hydrophobic nature of hydrogenated DDs and to investigate the hydration structure of AD and the DDs diamantane (DI), triamantane (TR), and hexamantane (HE). For this, we first calculate and characterize a realistic benchmark structure of the hydration shell around an AD molecule from DFT. We then simulate the same system with the ReaxFF parameter sets of Aryanpour,[47] Wang,[65] and Zhang[66] and compare the results against the benchmarks. Since it turns out that none of these force fields satisfactorily reproduces our references, we will adjust the Zhang parameter set to the DFT results by tuning its QEq parameters. After that, we extrapolate the modified force field to the other DDs and to room temperature in bulk water at normal conditions to predict their hydration structure.

2. METHODS

2.1. DFT Calculations. We first construct 21 random initial geometries of a single AD molecule surrounded by a shell of 143 water molecules (and also ten geometries of a single DI, TR, and HE each surrounded by 160 water molecules) with a procedure that we describe in the Supporting Information (section S5). Next, we optimize the initial geometries using the ORCA quantum chemistry program package[67,68] version 4.2.1. We employ the revPBE functional[69,70] and the def2-SVP basis set[71,72] with dispersion correction[73] while using loose optimization criteria. The functional is no hybrid functional and the basis set is relatively small, yet the lack of detail is a necessary compromise for optimizing bigger geometries and the method has proven itself before.[70,74] One geometry-optimized structure is depicted in Figure 1 both with the full water

https://doi.org/10.1021/acs.jpcc.2c07777
J. Phys. Chem. C 2023, 127, 3217−3227

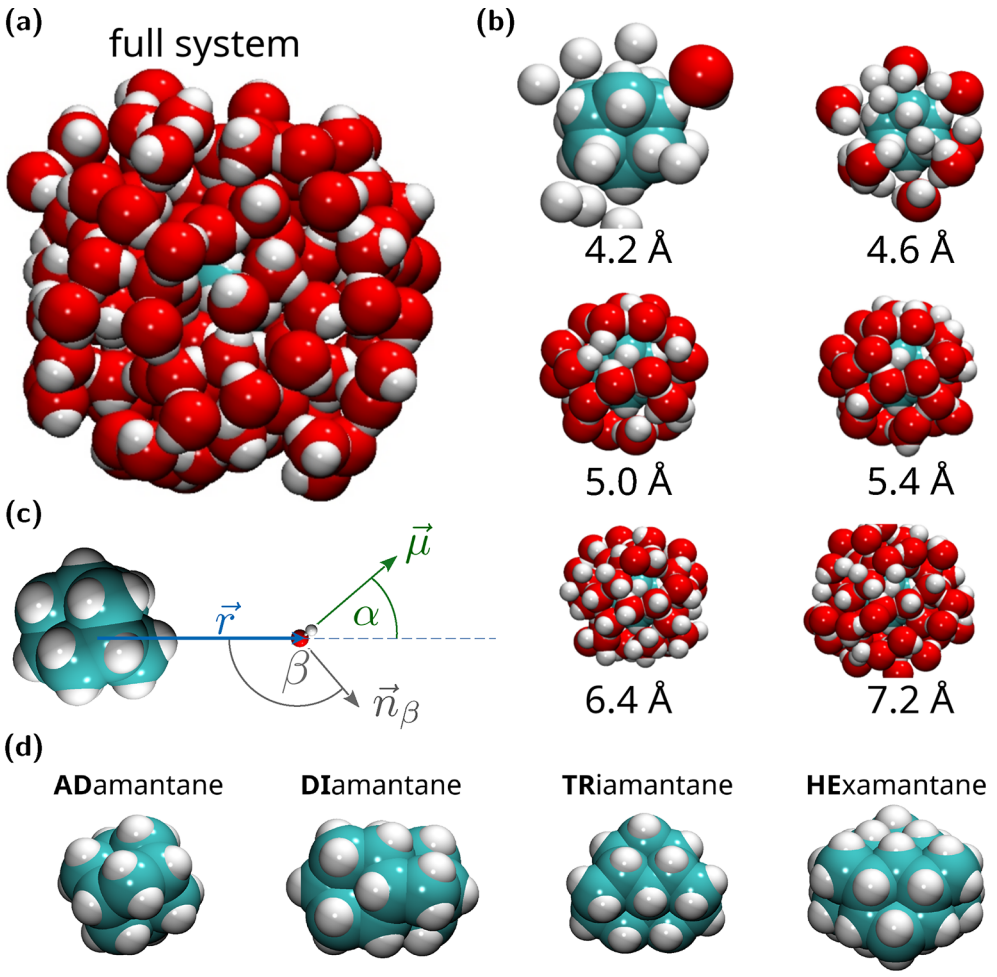

Figure 1. Illustrations of the simulated DD−water systems and important structural parameters. (a) The adamantane (AD) surrounded by a droplet of 143 water molecules, optimized with the revPBE functional and def2-SVP basis set with dispersion correction. (b) To illustrate the hydration-shell structure, the smaller pictures show the same system but the water atoms are cut off from view if their distance $|\vec{r}|$ to the AD center-of-mass (COM) is larger than the displayed value. (c) Illustration of the angles and vectors that describe the position and orientation of a water molecule relative to the AD COM. The angle α is defined between the water dipole moment vector $\vec{\mu}$ and the vector $\vec{r}$ connecting the AD COM to the water oxygen. The angle β is defined between the normal of the water molecular plane, $\vec{n}_\beta$, and the vector $\vec{r}$. (e) MD snapshots of the diamondoids considered in this study: adamantane ("AD", $C_{10}H_{16}$), diamantane ("DI", $C_{14}H_{20}$), triamantane ("TR", $C_{18}H_{24}$), and hexamantane ("HE", $C_{26}H_{30}$).

environment (panel a) and with only sublayers of the same (panel b). The structures are then analyzed to identify properties that can be used as benchmarks to compare different MD force fields.

2.2. MD Minimization with Existing ReaxFF Force Fields. After establishing our DFT benchmarks, we proceed with MD simulations. We perform MD energy minimization with a damped dynamics algorithm[75] at T = 0 K using the ReaxFF force field with the different parameter sets of Aryanpour,[47] Wang,[65] and Zhang.[66] With each parameter set, we minimize all 21 previously geometry-optimized AD+water structures. The simulations are computationally inexpensive; however, they do not exhaustively sample the phase space, so the results cannot make any statement about the statistical probability of the configurations. Regardless, as long as the DFT structures are representative of stable states in the MD simulations, then the structures should change as little as possible during the minimization. After that, we compare the MD-minimized structures to the DFT-optimized structures in terms of the benchmark properties.

2.3. Fitting of the Force Field Parameters. We modify the Zhang parameter set such that the MD-minimized structures achieve the optimal agreement with the DFT-optimized structures with respect to the benchmarks. We choose the Zhang set for its strength in regard to water simulations.[66] A full optimization of all ReaxFF force field parameters is, however, outside of the scope of this study. For the modifications, we tune the parameters associated with the QEq charge equilibration for the carbon atoms of the AD: The QEq method is based on the electronegativity equalization principle which states that, at equilibrium, the electron density transfers between all atoms such that the electronegativities at all atomic sites are equal.[48] The combination of partial charges that fulfills this condition is found by minimizing the electrostatic energy of the system after every reasonable number of time steps. There are three QEq parameters: the shielding, the electronegativity, and the hardness. We tune the shielding value in the range 0.1−1 $Å^{-1}$ with steps of 0.025 $Å^{-1}$, the electronegativity value in the range 1−12 eV with steps of 0.25 eV, and the hardness value in the range 1−8 eV with steps of 1 eV. For each parameter combination, we again minimize the previously DFT-optimized structures and calculate the averaged values for the benchmark properties. To find the optimal parameter set, we minimize the cost function

https://doi.org/10.1021/acs.jpcc.2c07777
J. Phys. Chem. C 2023, 127, 3217−3227

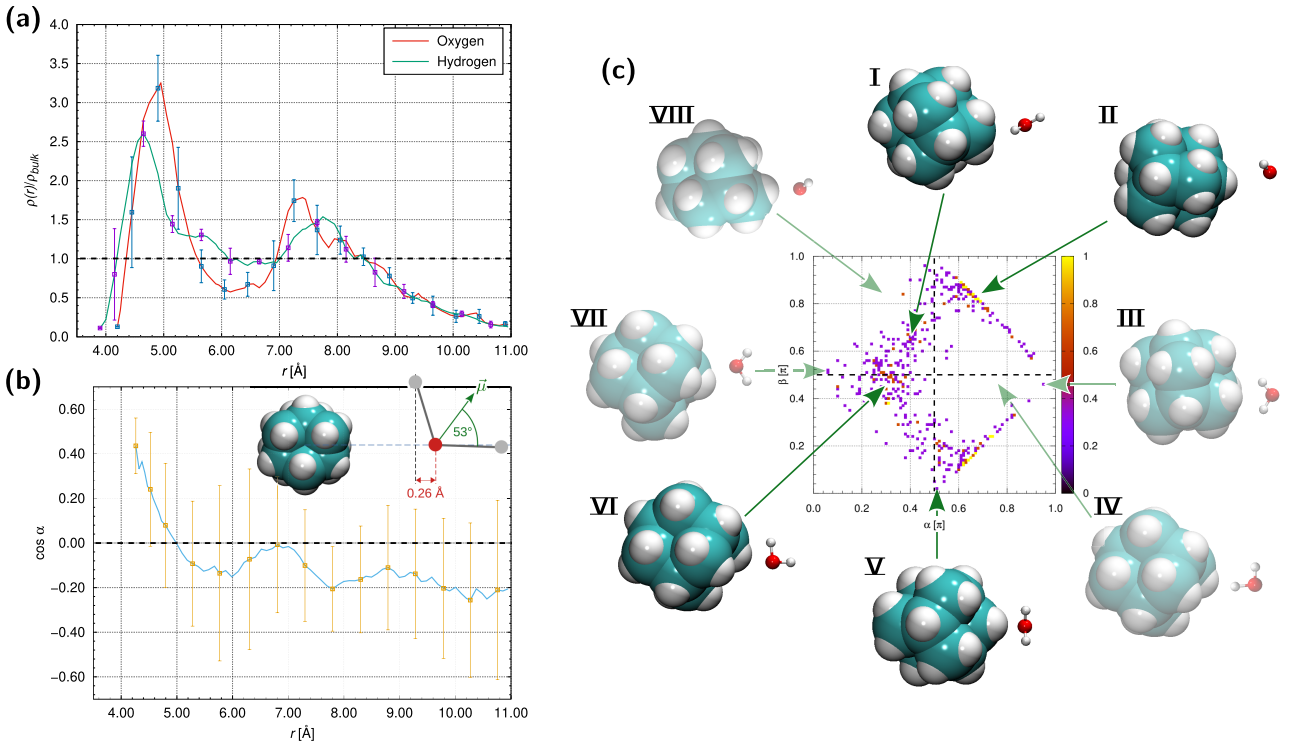

Figure 2. Results of the DFT geometry optimization of an AD surrounded by a droplet of 143 water molecules employing the revPBE functional and def2-SVP basis set with dispersion correction. (a) The radial density of the water O and H atoms as a function of the distance to the AD COM, normalized by the bulk density, 0.03344 Å^{-3} for O and 0.06688 Å^{-3} for H. (b) The orientation of the water dipole moments as a function of the distance to the AD COM. The error bars in (a) and (b) are the standard deviations from a set of 21 geometries after optimization. The inset illustrates a water molecule with $\alpha = 53°$, which is the average orientation closest to the AD. The illustration explains why the first peak of the H atom density is 0.26 Å closer to the AD than that of the C atom density. (c) The relationship between the angles α and β observed in the DFT-optimized structures in the first hydration shell. The color map indicates a relative probability for a molecule to occupy a certain (α, β) state. By dividing the map into sections, we can distinguish between eight types of similarly oriented water molecules which we call orientational modes.

$$\delta x = \sum_i \left[\frac{x_i^{\mathrm{DFT}} - x_i^{\mathrm{ReaxFF}}}{\sigma_i} \right]^2 \quad (1)$$

where x_i^{DFT} are the values of the benchmark quantities from the DFT calculations and x_i^{ReaxFF} are their counterparts from the MD simulations. The coefficient σ_i gives each benchmark quantity a weight, necessary to balance the influence that each quantity has on the cost function. This is an upper tolerance limit for the differences between the DFT and MD results. The weights are all about 10% of the maximum value of the corresponding benchmark quantities from the DFT optimization range. The parameter set which yields energy-minimized structures that minimize the cost function is next used to predict the water structure around the AD in bulk water at room temperature (T = 300 K).

2.4. MD Simulations at Room Temperature. Next, we prepare the simulations of an AD molecule solvated in bulk water. We use a cubic simulation box with periodic boundary conditions. We first fill the box with 343 water molecules and equilibrate them for 10 ps in the *NVT* ensemble at T = 300 K and at a particularly low density of 0.5 g/cm^3 so that we can later insert an AD molecule into the box without its atoms overlapping with water molecules. This way we mostly avoid having to remove water molecules from the simulation box so we do not have to replenish the box after the insertion of the solute to keep the number of water molecules approximately the same in all the following bulk simulations. We separately pre-equilibrate the AD molecule in a vacuum without periodic boundary conditions and then insert it into the water box so that the center-of-mass (COM) of the AD coincides with the center of the box. If the AD is still overlapping with water molecules, these molecules are removed from the simulation. In the subsequent equilibration in the *NPT* ensemble, the temperature and pressure are controlled by a Nosé−Hoover thermostat and barostat. They are set to T = 300 K and P = 1 atm, while the damping constants are set to 25 and 250 fs, respectively. The time step is 1 fs. Meanwhile, the AD is retained in the box center by subtracting the COM velocity of the AD from all atoms in the system. The equilibration is finished after 3 ns, when the total density becomes constant and slightly above 1 g/cm^3, and the mean value of the total energy does not change anymore. The production simulation runs for 1.5 ns with a time step of 0.5 fs.

3. RESULTS AND DISCUSSION

3.1. DFT Calculations. We summarize the results of the DFT geometry optimizations of the water droplets around the DDs. As a basis for comparing to structures that we will obtain from MD simulations, we define a set of benchmark quantities that characterize the alignment of the water molecules around the AD.

The first quantity is the radial density distribution of the water O and H atoms as a function of the distance r to the AD COM (Figure 2a). In the first hydration shell, which stretches from 4 to 6.2 Å (as defined by the first minimum of the O density), the water H atoms tend to rest 0.3 Å closer to the AD than the O atoms (see also Figure 1b). Above 6.2 Å, the region between the

https://doi.org/10.1021/acs.jpcc.2c07777
J. Phys. Chem. C 2023, 127, 3217−3227

Table 1. Time Averaged Total Number of DD−Water Dipole Bonds (C−H···O−H$_2$) and the Net Charges of the Investigated DDs, from the DFT Optimization and after MD Minimization with the Modified Zhang Parameters[a]

	dipole bonds				DD net charge [e]			
	AD	DI	TR	HE	AD	DI	TR	HE
DFT 0 K	1.3	0.2	0.6	2.3	−0.183	−0.133	−0.13	−0.21
MD 0 K	1.7	0.4	1.0	1.7	−0.197	−0.251	−0.127	0.303
MD 300 K	0.4	0.3	0.3	0.6	−0.298	−0.297	−0.185	0.188

[a]We also list the surface charge densities in the Supporting Information (section S6).

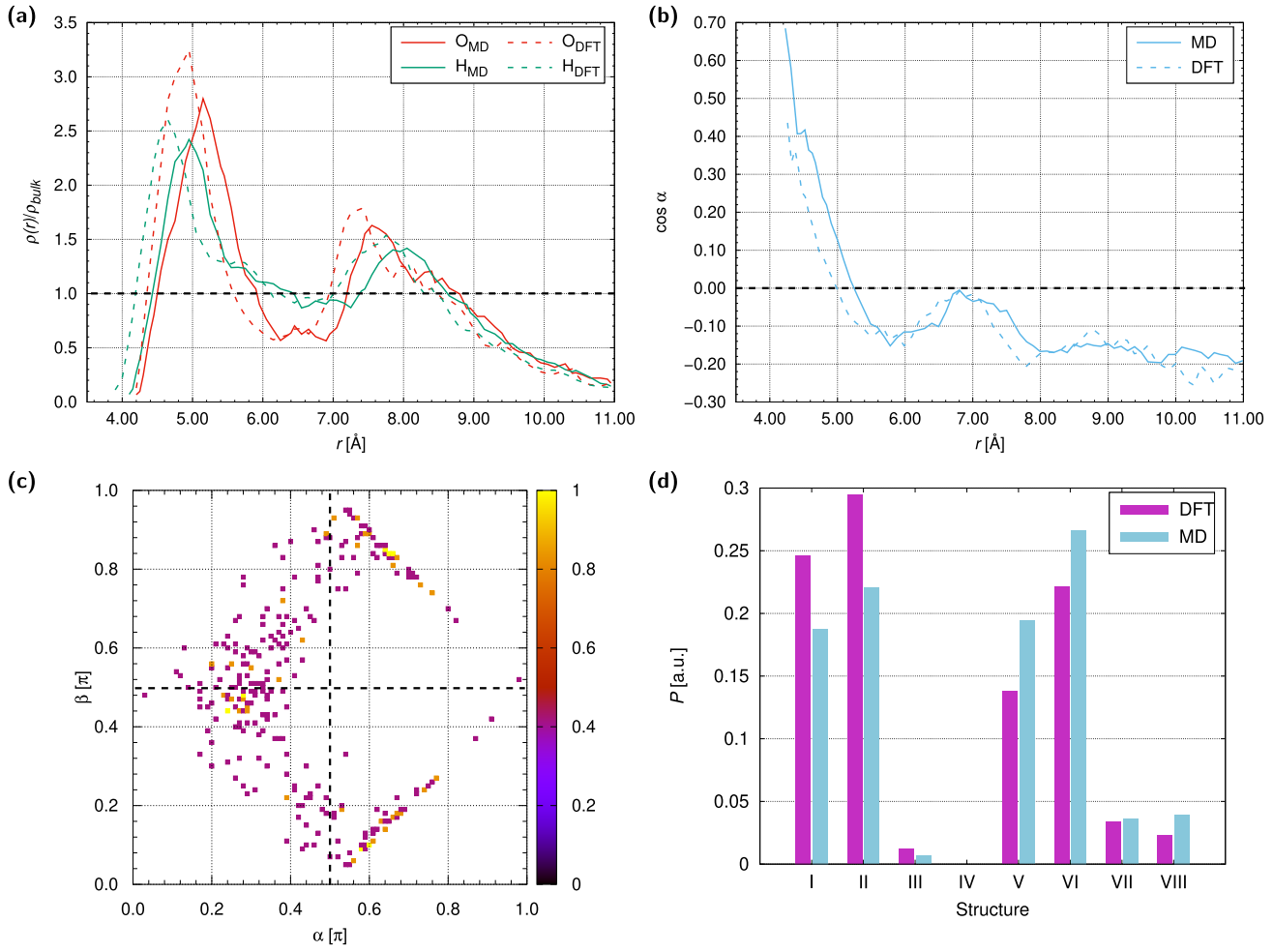

Figure 3. Summary of the 0 K minimization with the ReaxFF force field using the modified Zhang parameters. Comparison between the MD results and the DFT benchmarks. (a) The radial density of the water O and H atoms as a function of the distance to the AD COM, normalized by the bulk density, 0.03344 Å^{-3} for O and 0.06688 Å^{-3} for H. (b) The orientation of the water dipole moments as a function of the distance to the AD COM. (c) The relationship between the angles α and β in the first hydration shell obtained with the modified Zhang parameters. (d) The probabilities to find a water molecule in one of the structural modes which are defined in Figure 2c.

two peaks of the water density distribution forms a 1 Å wide hydrogen-dominated layer (see also Figure 1b). Note that both densities go to zero at high r, because the optimized structures are droplets and not periodic bulk water.

The second quantity is the cosine of the orientation angle α of the water dipole moments $\vec{\mu}$ as a function of the distance to the AD COM as defined in Figure 1c. Each dipole moment vector $\vec{\mu}$ is pointing from the O atom to the space halfway between the H atoms. Figure 2b shows that, close to the AD, the average α value is 53°. As shown in the inset of Figure 2b, there is a range of geometries where $\alpha = 53°$ while one H atom is ∼0.26 Å closer to the AD COM than the O atom. This explains the relative shift between the O and H peak in Figure 2a.

For the third benchmark quantity, we additionally introduce the angle β between the normal of the water molecular plane and $\vec{r}$ (see Figure 1c). In combination with the angle α, we obtain a detailed description of the alignment of the water molecules in the first hydration shell. Figure 2c shows the relationship between the angles α and β found in the DFT-optimized structures. The map can be divided up in sections, with each section corresponding to similarly oriented water molecules. For instance, the molecules corresponding to the top and bottom edges of that map ($\alpha \approx 0.5\pi, \beta \approx \pm 1\pi$) are aligned parallel to the AD surface, with only small variations, and the dipole directions are oriented tangential to the AD surface. The frequent occurrence of such oriented molecules is consistent with

https://doi.org/10.1021/acs.jpcc.2c07777
J. Phys. Chem. C 2023, 127, 3217−3227

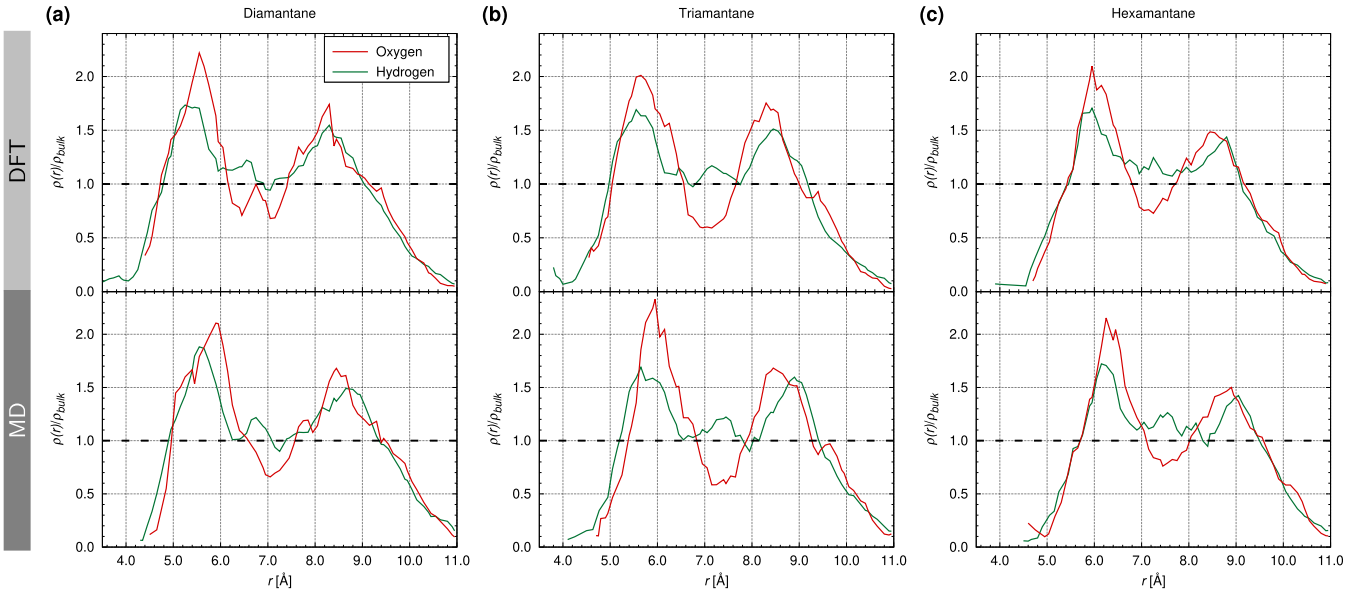

Figure 4. Radial density distributions of the water O and H atoms as a function of the distance to the diamondoid COM, normalized by the bulk density, 0.03344 $Å^{-3}$ for O and 0.06688 $Å^{-3}$ for H. The structures are composed of a diamondoid surrounded by a water droplet of 160 molecules. Comparison between DFT geometry optimization (top) and MD minimization with the modified Zhang parameters at T = 0 K (bottom).

previous Monte Carlo and MD simulations that used non polarizable force fields.[31,76] According to these studies, the water molecules in the first hydration shell are tangential to the skeleton surface of the AD. However, this is the single only orientational mode reported. Our simulations yield a spectrum of eight distinct modes of orientation, which we each number with a roman numeral. Many molecules occupy a bulge-like area close to the left edge of the map. These molecules are oriented as illustrated in the inset of Figure 2b. The other orientational modes are illustrated in Figure 2c. We identify modes I, II, V and VI, because they occur with a particularly high rate in the DFT results. Conversely, the other $\alpha-\beta$ combinations (modes III, IV, VII, and VIII) have a remarkably low occurrence on the map. The orientations of the water molecules are also related to the presence of non-hydrogen bonded OH groups in the first hydration shell, which is further discussed in the Supporting Information (section S4). The $\alpha-\beta$ map is a fingerprint of the water structure in the first hydration shell and serves as the third benchmark for the upcoming MD simulations.

The fourth quantity is the net charge of the AD. The net charges of the AD in the DFT calculations are determined with the ESP fit method and range from −0.356 e to +0.025 e with an average of −0.183 e. In accordance with previous investigations, there is a small electron transfer from water toward the AD.[77]

The fifth quantity is the number of C−H···O−H_2 dipole bonds (quasi hydrogen bonds) between the AD's H atoms and the water O atoms, where the C atoms are the donors and the water O atoms are the acceptors. We define a noncovalent bond as a dipole bond if the distance between the acceptor and the donor is lower than 3.5 Å and the C−H···O bond angle is smaller than 30°. The total number of AD−water dipole bonds in the DFT results, averaged over all configurations, is 1.3; i.e., only approximately 8% of the AD hydrogens are engaged in a dipole bond.

3.2. Benchmarking the ReaxFF Force Fields and Fitting to DFT. After the benchmarks have been established, we minimize the previously DFT-optimized structures using the ReaxFF force fields with the Aryanpour, Wang, and Zhang parameter sets. The deviations from the DFT-optimized structures are analyzed and presented in the Supporting Information (section S1).

We find that the commonly used ReaxFF parameters do not yield a good agreement with the DFT structures. The density distributions and orientations of the water molecules with respect to the AD COM are not correctly reproduced, the net charge of the AD is too high, and the number of AD−water dipole bonds is overestimated by a factor of ∼4. Thus, to fit the ReaxFF simulations to the DFT-optimized structures, it is necessary to modify one of the existing parameter sets. The procedure of fitting the QEq parameters that govern the charge equilibration of the C atoms is discussed in the Supporting Information (section S2).

We find that the cost function (eq 1) is minimized by QEq parameters that compromise on all benchmark quantities.

shielding	γ = 0.225 Å
electronegativity	χ = 7.00 eV
hardness	η = 7.0601 eV

The electronegativity corresponds to 2.788 on the Pauling scale and is close to the value for an isolated C atom (2.55) and much closer than the default value from the original Zhang parameter set (1.819). The net charges and number of AD−water dipole bonds are summarized in Table 1. The water O and H atom density distributions and the orientations of the water molecules are compared in Figure 3. The now modified Zhang parameter set generally overestimates the distances between the AD and the water molecules by 0.2−0.4 Å, but the relative distance between the O and the H distribution is consistent with the benchmarks (panel a). The angles of the water dipole moments are slightly overestimated on average but reproduce the orientations of the water molecules quite well, including the slope of cos(α) in the first hydration shell (panel b). We sometimes find molecules with a relatively high cos(α) value of approximately 0.7 at 4.2 Å, but their number is not statistically significant. The relationship between the α and β angles in the

https://doi.org/10.1021/acs.jpcc.2c07777
J. Phys. Chem. C 2023, 127, 3217−3227

first hydration shell is shown in panel c. In the form of a map, the angles are difficult to compare between MD and DFT, so we group the data into the orientational modes to help us interpret the hydration structure. Panel d shows the probability of a water molecule to be in one of the eight orientational modes. We see that in the MD-minimized structures it is 25% less probable to find a water molecule in modes I to III, compared to the DFT-optimized structures, while modes V to VIII have a 25% higher probability in MD than in DFT. However, the qualitative trends from the DFT benchmarks are all maintained upon MD minimization.

To further validate the new parameter set, we analyze whether the force field extrapolates to different DDs without loss of accuracy. We use the new parameter set to minimize DFT-optimized structures of a DI, a TR, and a HE molecule, each surrounded by 160 water molecules. For this, we apply the same DFT and MD methods as described in sections 2.1 and 2.2 (but with 10 structures per molecule). In Figure 4, we compare the MD-minimized structures to the DFT-optimized structures in terms of the water O and H density distributions. As with AD, we see a 0.2−0.4 Å shift between the DFT and the MD results, but the relative distributions between O and H are the same. Furthermore, in Table 1 we compare the MD-minimized structures to the DFT-optimized structures in terms of the number of weak DD−water dipole bonds and the DD net charges. In the case of DI and TR, the results are consistent with the AD results. As for HE, however, our modified Zhang parameter set overestimates the net charge. Thus, the analysis shows that the force field trained on AD successfully extrapolates to the larger DDs DI and TR, but further modifications may be needed when attempting to simulate larger structures.

3.3. MD Simulations at Room Temperature. The ReaxFF force field with the modified Zhang parameters for the C atoms is now used to investigate the water structure around the DDs which are each hydrated in bulk water at T = 300 K. Figure 5a shows the normalized density distributions of the water O and H atoms as a function of the distance to the DD COM. The results reflect typical signatures of hydrophobic solvation of smooth charged spheres, but with quantitative corrections.[78] From AD to TR, the heights of the first peaks decrease monotonically due to increasing attractive forces from the bulk. Also, each DDs O and H peaks are located at nearly the same distance from the DD's COM. However, the density distributions around the DDs show a weaker structuring compared to the smooth spheres at the same pressure and temperature. In the case of HE, the height of the first peaks increases again due to a compensating effect of the positive HE net charge (see Table 1). The water molecules respond by a cooperative reorientation, as indicated by the H peak shifting slightly away from the position of the O peak. Further corrections have their origin in the anisotropy of the DD's structures and small-scale interface effects.

Table 1 also shows that for all DDs the number of DD−water dipole bonds further decreases at room temperature compared to the results from MD minimization. This seems to indicate that C−H···O−H_2 dipole bonds are not disturbing the water hydrogen bond network surrounding the DDs. The few existing dipole bonds may even be a byproduct of the stabilization of the water hydrogen bond network very close to the interface, as we discuss in the Supporting Information (section S4). In Figure 6, we analyze the water structure of the first hydration shells around the DDs in more detail. The figure shows how the increase in molecular size affects the specific orientational modes

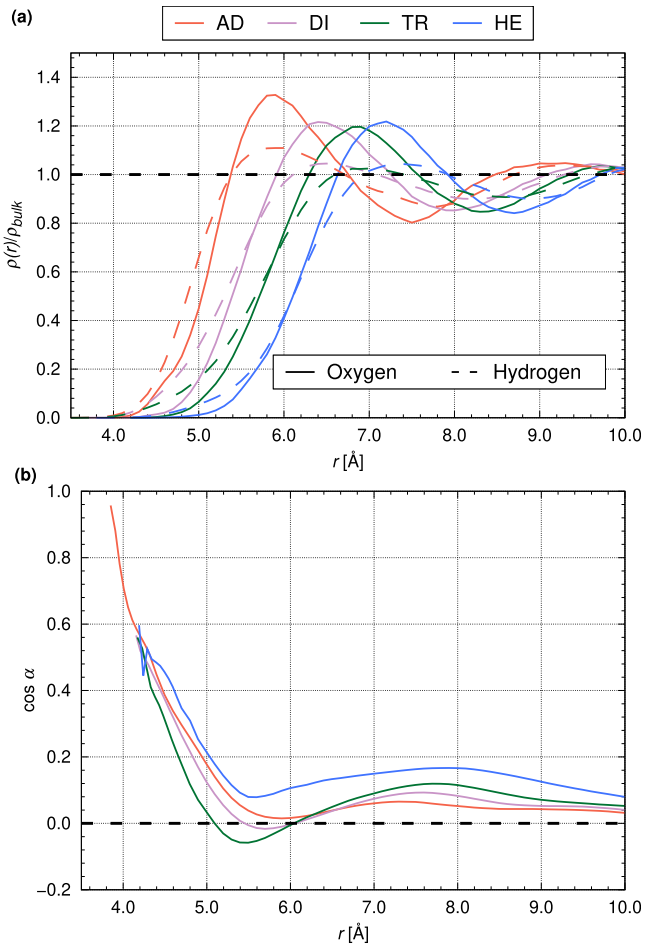

Figure 5. ReaxFF simulations of single diamondoids hydrated in bulk water at T = 300 K and P = 1 bar using the modified Zhang parameters. (a) The radial density distributions of the water O and H atoms as a function of the distance to the COM of the DDs, normalized by the bulk density, 0.03344 $Å^{-3}$ for O and 0.06688 $Å^{-3}$ for H. (b) The orientation of the water dipole moments as a function of the distance to the COM of the DDs.

of the water molecules in the first hydration shell. The blue lines show the results for the ReaxFF with the modified Zhang parameters. Every column corresponds to an orientational mode and the dots in each line stand for the DD, i.e., AD to HE from left to right. Every dot indicates the probability to find a water molecule oriented in the particular mode around the respective DD. With increasing DD size, we find a strong decrease of the probabilities of modes I and II, only small changes in modes III−VI, and a strong increase of modes VII and VIII. Generally, it becomes less likely for water molecules to point with their H atoms to the DD as the DD size increases. We suspect three reasons for this trend:

first, the change of the DD net charge (see Table 1)
second, the decrease of the DD curvature with increasing DD size
third, effects on small length scales at the DD−water interfaces due to the discrete partial charges

We can isolate the first two contributions from the third one by repeating the simulations with Lennard-Jones smooth spheres (SMS) instead of the DDs. For this, we replace the DD in our simulations by a Lennard-Jones particle with size σ_{SMS} and charge q_{SMS}. The mass m_{SMS} is the sum of the DD's

https://doi.org/10.1021/acs.jpcc.2c07777
J. Phys. Chem. C 2023, 127, 3217−3227

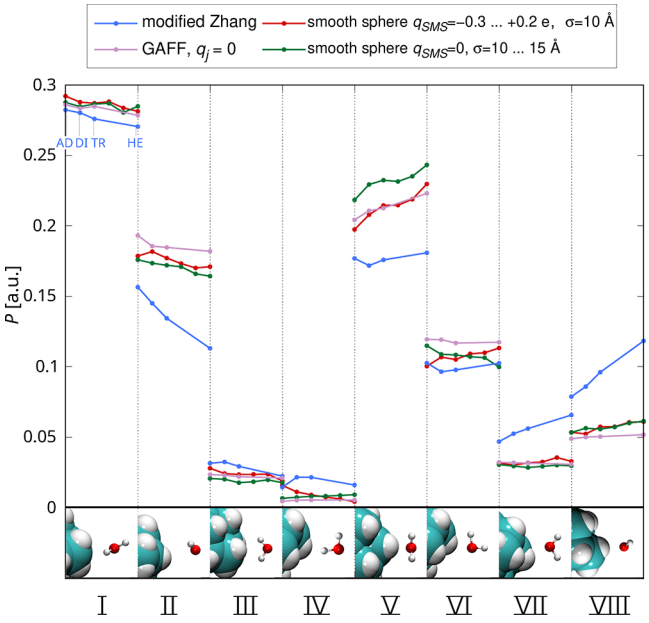

Figure 6. Probability of finding a water molecule in the first hydration shell to be oriented in one of the eight orientational modes. In the atomistic simulations (blue and purple lines), the dots in each line represent the diamondoids, AD to HE, from left to right. In the simulations with GAFF, all partial charges of the DDs were set to zero. In the simulations with smooth spheres (SMSs) instead of atomistic DDs, the dots represent different net charges q_{SMS} (red lines) and different sizes σ_{SMS} (green lines) of the SMSs, all of which correspond to the atomistic DDs. All simulations are at T = 300 K.

constituent atomic masses (e.g., m_{SMS} = 386.529 amu for AD), and ε_{SMS} = 0.11 kcal/mol, which is the same value used to simulate aliphatic carbon atoms in the General Amber Force Field (GAFF).[79] We compare the results from simulations with different σ_{SMS} and q_{SMS}, to find out which of those properties causes the strongest change of the water orientations in the first hydration shell.

For the simulations with different σ_{SMS}, the charge of the SMS is set to zero, but the size is varied from σ_{SMS} = 10 to 15 Å in steps of 1 Å. To determine which σ_{SMS} corresponds to which DD, we match the density distributions of the water O atoms around the DDs to those around the SMSs. We particularly match the position where the density of the rising first peak reaches the bulk value of 0.03344 $Å^{-3}$.

For the simulations with different q_{SMS}, the size of the hydrated SMSs is the AD size (σ_{SMS} = 10 Å) and the charges range between q_{SMS} = −0.3 e and +0.2 e in steps of 0.1 e, since the DD charges obtained with the modified Zhang parameters range from −0.2979 e (AD) to +0.1874 e (HE). To ensure charge neutrality, we compensate the solute charge by adding a counter charge to one randomly selected water molecule. We show in the Supporting Information (section S3.1) that, if a uniform background charge is applied instead, the differences in the results are negligible.

In Figure 6 (red and green lines), we review the eight specific orientational modes of the water molecules in the SMS simulations. In general, the probability to find a water molecule in each mode around a SMS is qualitatively similar to that of the corresponding DD from the atomistic simulation. Most of the upward and downward trends with increasing solute size also coincide, albeit with much smaller slopes, so that the water molecules are much stronger affected by the atomistic DDs than by the SMSs. We suspect that this is due to the distribution and strength of the partial charges of the DDs.

To confirm this, we resimulate the atomistic DDs but this time using GAFF and the TIP3P model for water, with all DD partial charges permanently set to zero. The response of the water molecules to the uncharged atomistic DDs (purple line in Figure 6) is just as weak as it is to the uncharged SMSs (green line). Apparently, the water molecules do not distinguish between the atomistic representation of a DD and an equivalently sized SMS, as long as both carry no charge. Neither do the water molecules respond particularly strongly to the change in the solute size as we see from the uncharged SMSs and from the uncharged GAFF model. Consequently, it must be the discrete distribution of partial charges in the modified Zhang model which strongly interact with the water molecules on small length scales.

We show in the Supporting Information (section S3) that there is also a connection between the changes in the water structure and the electrostatic potential inside the water, which confirms that the water distribution in hydrophobic hydration is affected by the complex electrostatic interactions between individual DD and water atoms on small length scales.

Lastly, we show in the Supporting Information (section S4) that these interactions are also responsible for the particular distribution of non-hydrogen bonded OH groups in the first hydration shells.

4. CONCLUSIONS

The goals of this work were to readjust a ReaxFF force field for MD simulations of DDs and to characterize their hydration structure in more detail than has ever been done before. We reviewed ReaxFF force fields from the literature[47,65,66] and realized that they do not yield simulation results that are consistent with our DFT benchmarks. Thus, we proposed a ReaxFF force field with refitted QEq parameters.

ReaxFF employs polarizable partial charges that describe many-particle interactions on small length scales more accurately than fixed partial charges do. This allowed us to shed new light on the electrostatic properties of the first hydration shell and its structure, which has been described as very unusual in experiments.[16] We found a spectrum of water orientations, greatly expanding on what was known before in literature.[31,76] We showed that there are almost no interfacial C−H···O−H_2 bonds, in which we agree with experiments,[16] except at very close distances to the interface, where they contribute to the stabilization of the water−water hydrogen bond network.[23] However, we also showed that there is a substantial number of non-hydrogen bonded OH groups within the first hydration shell, which have also been observed around NDs and other hydrocarbons.[24,38−42] Generally, we found that for understanding hydrophobic hydration[80,81] it is of fundamental importance to know the effects of small surface perturbations on hydrophobic behavior. From the systematic exclusion of atomistic detail we can conclude that the hydration structure is strongly affected by the interactions between the discrete partial charges on small length scales at the DD−water interface. However, we can also conclude that hydrophobic behavior is qualitatively impervious to small surface perturbations.

Further work is underway to extend the model to simulate the interplay between dopants and electrolytes and to study surface transfer doping and the dynamics of solvated electrons generated from DDs and NDs. Our study may also motivate future investigations with a view to a better transferability of

https://doi.org/10.1021/acs.jpcc.2c07777
J. Phys. Chem. C 2023, 127, 3217−3227

ReaxFF force fields to a wider variety of hydrocarbon/water systems.

■ ASSOCIATED CONTENT

Supporting Information

The Supporting Information is available free of charge at https://pubs.acs.org/doi/10.1021/acs.jpcc.2c07777.

Comparison to existing ReaxFF force fields, energy minimization results, table of number of dipole bonds, fitting of the force field parameters, table of weighting coefficients, trends from the QEq parameter study, electrostatic properties of the bulk water around the hydrated DDs, charge neutrality in the smooth sphere simulations, non-hydrogen bonded OH groups in the first hydration shell, generation of the initial coordinates for the DFT optimization, surface charge densities, and table of SASAs and charge densities (PDF)

■ AUTHOR INFORMATION

Corresponding Authors

Karol Palczynski − *Research Group Simulations of Energy Materials, Helmholtz-Zentrum Berlin für Materialien und Energie, D-14109 Berlin, Germany;* orcid.org/0000-0003-2979-4281; Email: karol.palczynski@helmholtz-berlin.de

Thorren Kirschbaum − *Research Group Simulations of Energy Materials, Helmholtz-Zentrum Berlin für Materialien und Energie, D-14109 Berlin, Germany; Institute of Mathematics, Freie Universität Berlin, D-14195 Berlin, Germany;* Email: thorren.kirschbaum@helmholtz-berlin.de

Annika Bande − *Theory of Electron Dynamics and Spectroscopy, Helmholtz-Zentrum Berlin für Materialien und Energie, D-14109 Berlin, Germany;* orcid.org/0000-0003-3827-9169; Email: annika.bande@helmholtz-berlin.de

Joachim Dzubiella − *Applied Theoretical Physics - Computational Physics, Albert-Ludwigs-Universität Freiburg, D-79104 Freiburg, Germany; Research Group Simulations of Energy Materials, Helmholtz-Zentrum Berlin für Materialien und Energie, D-14109 Berlin, Germany;* orcid.org/0000-0001-6751-1487; Email: joachim.dzubiella@physik.uni-freiburg.de

Complete contact information is available at: https://pubs.acs.org/10.1021/acs.jpcc.2c07777

Notes

The authors declare no competing financial interest.

■ ACKNOWLEDGMENTS

The authors acknowledge support by the state of Baden-Württemberg through bwHPC and support from the high performance computing cluster Curta of Freie Universität Berlin (https://refubium.fu-berlin.de/handle/fub188/26993). T.K. and J.D. acknowledge the support of the Helmholtz Einstein International Berlin Research School in Data Science (HEIBRiDS). The authors wish to thank Dr. Sébastien Groh for his help with ReaxFF and inspiring discussions.

■ REFERENCES

(1) Ge, Z.; Li, Q.; Wang, Y. Free Energy Calculation of Nanodiamond-Membrane Association—The Effect of Shape and Surface Functionalization. *J. Chem. Theory Comput.* **2014**, *10*, 2751−2758.

(2) Henych, J.; Stehlík, Š.; Mazanec, K.; Tolasz, J.; Čermák, J.; Rezek, B.; Mattsson, A.; Österlund, L. Reactive adsorption and photodegradation of soman and dimethyl methylphosphonate on TiO2/nanodiamond composites. *Appl. Catal., B* **2019**, *259*, 118097.

(3) Khajeh, A.; Krim, J.; Martini, A. Synergistic effect of nanodiamonds on the adsorption of tricresyl phosphate on iron oxide surfaces. *Appl. Phys. Lett.* **2019**, *114*, 171602.

(4) Aranifard, S.; Shojaei, A. Chitosan interphase around nanodiamond: Insight from equilibrium molecular dynamics. *Diam. Relat. Mater.* **2020**, *104*, 107737.

(5) Yeung, K.-W.; Dong, Y.; Chen, L.; Tang, C.-Y.; Law, W.-C.; Tsui, G. C.-P. Nanotechnology of diamondoids for the fabrication of nanostructured systems. *Nanotechnol. Rev.* **2020**, *9*, 650−669.

(6) Miliaieva, D.; Matunova, P.; Cermak, J.; Stehlik, S.; Cernescu, A.; Remes, Z.; Stenclova, P.; Muller, M.; Rezek, B. Nanodiamond surface chemistry controls assembly of polypyrrole and generation of photovoltage. *Sci. Rep.* **2021**, *11*, 590.

(7) Mochalin, V. N.; Shenderova, O.; Ho, D.; Gogotsi, Y. The properties and applications of nanodiamonds. *Nat. Nanotechnol.* **2012**, *7*, 11−23.

(8) Lamoureux, G.; Artavia, G. Use of the Adamantane Structure in Medicinal Chemistry. *Curr. Med. Chem.* **2010**, *17*, 2967−2978.

(9) Mansoori, G. A. Diamondoids − The Molecular Lego of Biomedicine, Materials Science and Nanotechnology. *J. Bioanal. Biomed.* **2013**, *05*, 2.

(10) Jariwala, D. H.; Patel, D.; Wairkar, S. Surface functionalization of nanodiamonds for biomedical applications. *Mater. Sci. Eng., C* **2020**, *113*, 110996.

(11) Dahl, J. E.; Liu, S. G.; Carlson, R. M. K. Isolation and Structure of Higher Diamondoids, Nanometer-Sized Diamond Molecules. *Science* **2003**, *299*, 96−99.

(12) Stehlik, S.; Glatzel, T.; Pichot, V.; Pawlak, R.; Meyer, E.; Spitzer, D.; Rezek, B. Water interaction with hydrogenated and oxidized detonation nanodiamonds — Microscopic and spectroscopic analyses. *Diam. Relat. Mater.* **2016**, *63*, 97−102.

(13) Machova, I.; Hubalek, M.; Belinova, T.; Fucikova, A.; Stehlik, S.; Rezek, B.; Kalbacova, M. H. The bio-chemically selective interaction of hydrogenated and oxidized ultra-small nanodiamonds with proteins and cells. *Carbon* **2020**, *162*, 650−661.

(14) Horinek, D.; Serr, A.; Bonthuis, D. J.; Boström, M.; Kunz, W.; Netz, R. R. Molecular Hydrophobic Attraction and Ion-Specific Effects Studied by Molecular Dynamics. *Langmuir* **2008**, *24*, 1271−1283.

(15) Petit, T.; Yuzawa, H.; Nagasaka, M.; Yamanoi, R.; Osawa, E.; Kosugi, N.; Aziz, E. F. Probing Interfacial Water on Nanodiamonds in Colloidal Dispersion. *J. Phys. Chem. Lett.* **2015**, *6*, 2909−2912.

(16) Petit, T.; Puskar, L.; Dolenko, T.; Choudhury, S.; Ritter, E.; Burikov, S.; Laptinskiy, K.; Brzustowski, Q.; Schade, U.; Yuzawa, H.; et al. Unusual Water Hydrogen Bond Network around Hydrogenated Nanodiamonds. *J. Phys. Chem. C* **2017**, *121*, 5185−5194.

(17) Ji, S.; Jiang, T.; Xu, K.; Li, S. FTIR study of the adsorption of water on ultradispersed diamond powder surface. *Appl. Surf. Sci.* **1998**, *133*, 231−238.

(18) Dolenko, T. A.; Burikov, S. A.; Rosenholm, J. M.; Shenderova, O. A.; Vlasov, I. I. Diamond−Water Coupling Effects in Raman and Photoluminescence Spectra of Nanodiamond Colloidal Suspensions. *J. Phys. Chem. C* **2012**, *116*, 24314−24319.

(19) Batsanov, S. S.; Lesnikov, E. V.; Dan'kin, D. A.; Balakhanov, D. M. Water shells of diamond nanoparticles in colloidal solutions. *Appl. Phys. Lett.* **2014**, *104*, 133105.

(20) Galamba, N. Water's Structure around Hydrophobic Solutes and the Iceberg Model. *J. Phys. Chem. B* **2013**, *117*, 2153−2159.

(21) Graziano, G. Comment on "Water's Structure around Hydrophobic Solutes and the Iceberg Model. *J. Phys. Chem. B* **2014**, *118*, 2598−2599.

(22) Maciel, C.; Malaspina, T.; Fileti, E. E. Prediction of the Hydration Properties of Diamondoids from Free Energy and Potential of Mean Force Calculations. *J. Phys. Chem. B* **2012**, *116*, 13467−13471.

(23) Saberi-Movahed, F.; Brenner, D. W. Impacts of surface chemistry and adsorbed ions on dynamics of water around detonation nanodiamond in aqueous salt solutions. *arXiv (Computational Physics,*

Soft Condensed Matter, Chemical Physics) **2021**, DOI: 10.48550/ARXIV.2102.13312. (accessed September 21, 2021)
(24) Saberi-Movahed, F.; Brenner, D. W. What drives adsorption of ions on surface of nanodiamonds in aqueous solutions? *arXiv (Computational Physics)* **2021**, DOI: 10.48550/ARXIV.2102.09187. (accessed September 21, 2021)
(25) Saberi-Movahed, F.; Brenner, D. W. Atomistic insights into hydrogen bonds of water around detonation nanodiamonds: effects of surface chemistry and dissolved ions. *arXiv (Computational Physics)* **2021**, DOI: 10.48550/ARXIV.2103.01385. (accessed September 21, 2021)
(26) Chew, C. F.; Guy, A.; Biggin, P. C. Distribution and Dynamics of Adamantanes in a Lipid Bilayer. *Biophys. J.* **2008**, *95*, 5627−5636.
(27) Ge, Z.; Wang, Y. Estimation of Nanodiamond Surface Charge Density from Zeta Potential and Molecular Dynamics Simulations. *J. Phys. Chem. B* **2017**, *121*, 3394−3402.
(28) Vanommeslaeghe, K.; Raman, E. P.; MacKerell, A. D. Automation of the CHARMM General Force Field (CGenFF) II: Assignment of Bonded Parameters and Partial Atomic Charges. *J. Chem. Inf. Model.* **2012**, *52*, 3155−3168.
(29) Schönbeck, C. Charge Determines Guest Orientation: A Combined NMR and Molecular Dynamics Study of *β*-Cyclodextrins and Adamantane Derivatives. *J. Phys. Chem. B* **2018**, *122*, 4821−4827.
(30) Wang, M.; Zhang, K.; Hou, D.; Wang, P. Microscopic insight into nanodiamond polymer composites: reinforcement, structural, and interaction properties. *Nanoscale* **2020**, *12*, 24107−24118.
(31) Ohisa, M.; Aida, M. Solvent distributions, solvent orientations and specific hydration regions around 1-adamantyl chloride and adamantane in aqueous solution. *Chem. Phys. Lett.* **2011**, *511*, 62−67.
(32) Makowski, M.; Czaplewski, C.; Liwo, A.; Scheraga, H. A. Potential of Mean Force of Association of Large Hydrophobic Particles: Toward the Nanoscale Limit. *J. Phys. Chem. B* **2010**, *114*, 993−1003.
(33) Bogunia, M.; Liwo, A.; Czaplewski, C.; Makowska, J.; Giełdoń, A.; Makowski, M. Influence of Temperature and Salt Concentration on the Hydrophobic Interactions of Adamantane and Hexane. *J. Phys. Chem. B* **2022**, *126*, 634−642.
(34) Karásek, P.; Planeta, J.; Roth, M. Solubilities of Adamantane and Diamantane in Pressurized Hot Water. *J. Chem. Eng. Data* **2008**, *53*, 816−819.
(35) Harries, D.; Rau, D. C.; Parsegian, V. A. Solutes Probe Hydration in Specific Association of Cyclodextrin and Adamantane. *J. Am. Chem. Soc.* **2005**, *127*, 2184−2190.
(36) Taulier, N.; Chalikian, T. V. Hydrophobic Hydration in Cyclodextrin Complexation. *J. Phys. Chem. B* **2006**, *110*, 12222−12224.
(37) Assaf, K. I.; Florea, M.; Antony, J.; Henriksen, N. M.; Yin, J.; Hansen, A.; Qu, Z.; Sure, R.; Klapstein, D.; Gilson, M. K.; et al. HYDROPHOBE Challenge: A Joint Experimental and Computational Study on the Host−Guest Binding of Hydrocarbons to Cucurbiturils, Allowing Explicit Evaluation of Guest Hydration Free-Energy Contributions. *J. Phys. Chem. B* **2017**, *121*, 11144−11162.
(38) Mizuno, K.; Masuda, Y.; Yamamura, T.; Kitamura, J.; Ogata, H.; Bako, I.; Tamai, Y.; Yagasaki, T. Roles of the Ether Oxygen in Hydration of Tetrahydrofuran Studied by IR, NMR, and DFT Calculation Methods. *J. Phys. Chem. B* **2009**, *113*, 906−915.
(39) Perera, P. N.; Fega, K. R.; Lawrence, C.; Sundstrom, E. J.; Tomlinson-Phillips, J.; Ben-Amotz, D. Observation of water dangling OH bonds around dissolved nonpolar groups. *Proc. Natl. Acad. Sci. U. S. A.* **2009**, *106*, 12230−12234.
(40) Tomlinson-Phillips, J.; Davis, J.; Ben-Amotz, D.; Spångberg, D.; Pejov, L.; Hermansson, K. Structure and Dynamics of Water Dangling OH Bonds in Hydrophobic Hydration Shells. Comparison of Simulation and Experiment. *J. Phys. Chem. A* **2011**, *115*, 6177−6183.
(41) Davis, J. G.; Gierszal, K. P.; Wang, P.; Ben-Amotz, D. Water structural transformation at molecular hydrophobic interfaces. *Nature* **2012**, *491*, 582−585.
(42) Davis, J. G.; Rankin, B. M.; Gierszal, K. P.; Ben-Amotz, D. On the cooperative formation of non-hydrogen-bonded water at molecular hydrophobic interfaces. *Nat. Chem.* **2013**, *5*, 796−802.
(43) Hölzl, C.; Horinek, D. Pressure increases the ice-like order of water at hydrophobic interfaces. *Phys. Chem. Chem. Phys.* **2018**, *20*, 21257−21261.
(44) Scheiner, S. Weak H-bonds. Comparisons of CH···O to NH···O in proteins and PH···N to direct P···N interactions. *Phys. Chem. Chem. Phys.* **2011**, *13*, 13860.
(45) Kananenka, A. A.; Skinner, J. L. Unusually strong hydrogen bond cooperativity in particular $(H_2O)_{20}$ clusters. *Phys. Chem. Chem. Phys.* **2020**, *22*, 18124−18131.
(46) van Duin, A. C. T.; Dasgupta, S.; Lorant, F.; Goddard, W. A. ReaxFF: A Reactive Force Field for Hydrocarbons. *J. Phys. Chem. A* **2001**, *105*, 9396−9409.
(47) Aryanpour, M.; van Duin, A. C. T.; Kubicki, J. D. Development of a Reactive Force Field for Iron-Oxyhydroxide Systems. *J. Phys. Chem. A* **2010**, *114*, 6298−6307.
(48) Mortier, W. J.; Ghosh, S. K.; Shankar, S. Electronegativity-equalization method for the calculation of atomic charges in molecules. *J. Am. Chem. Soc.* **1986**, *108*, 4315−4320.
(49) Rappe, A. K.; Goddard, W. A. Charge equilibration for molecular dynamics simulations. *J. Phys. Chem.* **1991**, *95*, 3358−3363.
(50) Nakano, A. Parallel multilevel preconditioned conjugate-gradient approach to variable-charge molecular dynamics. *Comput. Phys. Commun.* **1997**, *104*, 59−69.
(51) Aktulga, H.; Fogarty, J.; Pandit, S.; Grama, A. Parallel reactive molecular dynamics: Numerical methods and algorithmic techniques. *Parallel Comput* **2012**, *38*, 245−259.
(52) Luzhkov, V.; Decroly, E.; Canard, B.; Selisko, B.; Åqvist, J. Evaluation of Adamantane Derivatives as Inhibitors of Dengue Virus mRNA Cap Methyltransferase by Docking and Molecular Dynamics Simulations. *Mol. Inform.* **2013**, *32*, 155−164.
(53) Chang, S. L. Y.; Dwyer, C.; Osawa, E.; Barnard, A. S. Size dependent surface reconstruction in detonation nanodiamonds. *Nanoscale Horiz* **2018**, *3*, 213−217.
(54) Mikheev, K. G.; Mogileva, T. N.; Fateev, A. E.; Nunn, N. A.; Shenderova, O. A.; Mikheev, G. M. Low-Power Laser Graphitization of High Pressure—High Temperature Nanodiamond Films. *Appl. Sci.* **2020**, *10*, 3329.
(55) Petit, T.; Arnault, J.-C.; Girard, H. A.; Sennour, M.; Kang, T.-Y.; Cheng, C.-L.; Bergonzo, P. Oxygen hole doping of nanodiamond. *Nanoscale* **2012**, *4*, 6792.
(56) Zhang, L.; Zhu, D.; Nathanson, G. M.; Hamers, R. J. Selective Photoelectrochemical Reduction of Aqueous CO_2 to CO by Solvated Electrons. *Angew. Chem.* **2014**, *126*, 9904−9908.
(57) Brun, E.; Girard, H. A.; Arnault, J.-C.; Mermoux, M.; Sicard-Roselli, C. Hydrogen plasma treated nanodiamonds lead to an overproduction of hydroxyl radicals and solvated electrons in solution under ionizing radiation. *Carbon* **2020**, *162*, 510−518.
(58) Buchner, F.; Kirschbaum, T.; Venerosy, A.; Girard, H.; Arnault, J.-C.; Kiendl, B.; Krueger, A.; Larsson, K.; Bande, A.; Petit, T. Early dynamics of the emission of solvated electrons from nanodiamonds in water. *Nanoscale* **2022**, *14*, 17188.
(59) Islam, M. M.; Kolesov, G.; Verstraelen, T.; Kaxiras, E.; van Duin, A. C. T. eReaxFF: A Pseudoclassical Treatment of Explicit Electrons within Reactive Force Field Simulations. *J. Chem. Theory Comput.* **2016**, *12*, 3463−3472.
(60) Gunawan, M. A.; Hierso, J.-C.; Poinsot, D.; Fokin, A. A.; Fokina, N. A.; Tkachenko, B. A.; Schreiner, P. R. Diamondoids: functionalization and subsequent applications of perfectly defined molecular cage hydrocarbons. *New J. Chem.* **2014**, *38*, 28−41.
(61) Larsson, K.; Tian, Y. Effect of surface termination on the reactivity of nano-sized diamond particle surfaces for bio applications. *Carbon* **2018**, *134*, 244−254.
(62) Jariwala, D. H.; Patel, D.; Wairkar, S. Surface functionalization of nanodiamonds for biomedical applications. *Mater. Sci. Eng.* **2020**, *113*, 110996.
(63) Kirschbaum, T.; Petit, T.; Dzubiella, J.; Bande, A. Effects of oxidative adsorbates and cluster formation on the electronic structure of nanodiamonds. *J. Comput. Chem.* **2022**, *43*, 923−929.

(64) Sanz-Navarro, C. F.; Åstrand, P.-O.; Chen, D.; Rønning, M.; van Duin, A. C. T.; Mueller, J. E.; III, W. A. G. Molecular Dynamics Simulations of Carbon-Supported Ni Clusters Using the Reax Reactive Force Field. *J. Phys. Chem. C* **2008**, *112*, 12663−12668.
(65) Wang, Y.; Shi, Y.; Sun, Q.; Lu, K.; Kubo, M.; Xu, J. Development of a Transferable ReaxFF Parameter Set for Carbon- and Silicon-Based Solid Systems. *J. Phys. Chem. C* **2020**, *124*, 10007−10015.
(66) Zhang, W.; van Duin, A. C. T. Improvement of the ReaxFF Description for Functionalized Hydrocarbon/Water Weak Interactions in the Condensed Phase. *J. Phys. Chem. B* **2018**, *122*, 4083−4092.
(67) Neese, F. The ORCA program system. *Wiley Interdiscip. Rev.: Comput. Mol. Sci.* **2012**, *2*, 73−78.
(68) Neese, F. Software update: the ORCA program system, version 4.0. *Wiley Interdiscip. Rev.: Comput. Mol. Sci.* **2018**, *8*, e1327.
(69) Zhang, Y.; Yang, W. Comment on "Generalized Gradient Approximation Made Simple. *Phys. Rev. Lett.* **1998**, *80*, 890−890.
(70) Gillan, M. J.; Alfè, D.; Michaelides, A. Perspective: How good is DFT for water? *J. Chem. Phys.* **2016**, *144*, 130901.
(71) Schäfer, A.; Horn, H.; Ahlrichs, R. Fully optimized contracted Gaussian basis sets for atoms Li to Kr. *J. Chem. Phys.* **1992**, *97*, 2571−2577.
(72) Weigend, F.; Ahlrichs, R. Balanced basis sets of split valence, triple zeta valence and quadruple zeta valence quality for H to Rn: Design and assessment of accuracy. *Phys. Chem. Chem. Phys.* **2005**, *7*, 3297−3305.
(73) Grimme, S.; Ehrlich, S.; Goerigk, L. Effect of the damping function in dispersion corrected density functional theory. *J. Comput. Chem.* **2011**, *32*, 1456−1465.
(74) Ganji, M. D.; Mirzaei, S.; Dalirandeh, Z. Molecular origin of drug release by water boiling inside carbon nanotubes from reactive molecular dynamics simulation and DFT perspectives. *Sci. Rep.* **2017**, *7*, 4669.
(75) Bitzek, E.; Koskinen, P.; Gähler, F.; Moseler, M.; Gumbsch, P. Structural Relaxation Made Simple. *Phys. Rev. Lett.* **2006**, *97*, 170201.
(76) Doi, H.; Aida, M. Hydration of Adamantane Skeleton: Water Assembling around Amantadine and Halo-substituted Adamantanes. *Chem. Lett.* **2013**, *42*, 292−294.
(77) Petrini, D.; Larsson, K. Electron Transfer from a Diamond (100) Surface to an Atmospheric Water Adlayer: A Quantum Mechanical Study. *J. Phys. Chem. C* **2007**, *111*, 13804−13812.
(78) Dzubiella, J.; Hansen, J.-P. Competition of hydrophobic and Coulombic interactions between nanosized solutes. *J. Chem. Phys.* **2004**, *121*, 5514−5530.
(79) Wang, J.; Wolf, R. M.; Caldwell, J. W.; Kollman, P. A.; Case, D. A. Development and testing of a general amber force field. *J. Comput. Chem.* **2004**, *25*, 1157−1174.
(80) Lum, K.; Chandler, D.; Weeks, J. D. Hydrophobicity at Small and Large Length Scales. *J. Phys. Chem. B* **1999**, *103*, 4570−4577.
(81) Chandler, D. Hydrophobicity: Two faces of water. *Nature* **2002**, *417*, 491−491.

https://doi.org/10.1021/acs.jpcc.2c07777
J. Phys. Chem. C 2023, 127, 3217−3227